Modeling Unsaturated Soil Column Collapse through Stabilized Updated Lagrangian Periporomechanics

Shashank Menon, Ph.D.¹; and Xiaoyu Song, Ph.D., M.ASCE²

¹Ph.D. Student, Dept. of Civil and Coastal Engineering, Univ. of Florida ²Associate Professor, Dept. of Civil and Coastal Engineering, Univ. of Florida (corresponding author). Email: xysong@ufl.edu

ABSTRACT

Soil column collapse has been widely studied in the dry condition due to its applicability to natural phenomena such as landslides, avalanches, and debris flows. Given the prevalence of unsaturated soils in nature, in this study, we apply a recently proposed nonlocal poromechanics formulation to study three-dimensional unsaturated soil column collapse. For accuracy and robustness in modeling large deformation and plasticity, an updated Lagrangian framework is adopted in which the equation of motion is formulated in the current/deformed configuration. Numerical simulations are conducted to explore the influence of aspect ratio of the column on the flow characteristics of unsaturated soil. The results are validated using experimental data of collapsed deposit morphology and final height. We also study the influence of initial matric suction in the soil on the final deposit shape.

INTRODUCTION

Geomaterials are composed of a skeleton made of individual grains that behave as rigid solids. Under large deformation and high strain gradients, they can exhibit fluid-like characteristics such as flow, high compressibility and negligible shear resistance. Under unsaturated conditions, geomaterials consist of three phases – solid skeleton, pore water and pore air. Unsaturated soil mechanics is of great interest to researchers in geological and geotechnical fields due to its applicability to phenomena such as debris flows and slope instability (Fredlund and Rahardjo, 1993; Lu and Likos 2004; Alonso 2021). Debris flows such as avalanches and mudslides are particularly common occurrence around the globe and can travel extensive distances, thus representing a major geohazard. These phenomena can be triggered by changes in matric suction. A particular problem that has received much research in physics and soil mechanics is the collapse of a granular column under the action of gravity. The collapse of granular material under gravity loads was studied experimentally (Lube et al., 2004; Lajeunesse et al., 2004). In the laboratory testing a mass of dry granular material densely packed in a glass tube was allowed to collapse under onto a horizontal bed under its own weight by rapid removal of the glass tube. The experimental results showed the existence of three different regimes of collapse, governed by the initial aspect ratio.

The dynamic collapse of granular columns has been investigated using continuum-based numerical approaches. For instance, the finite element method and material point method (Alonso, 2021) were used to study granular collapse dynamics in planar condition and its dependence on the internal friction angle of soil. A comprehensive review of numerical modeling of soil column collapse can be found in Menon and Song (2022b). Soil column collapse has been studied under fully dry condition (Fávero Neto and Borja 2018). Soil column collapse under

unsaturated conditions is not well studied. In this study, we present a numerical investigation of the unsaturated soil column collapse in three dimensions under drained conditions through a recently proposed unsaturated periporomechanics model (Menon and Song 2021).

FORMULATION

Periporomechanics is a strongly nonlocal reformulation of classical poromechanics that utilizes the peridynamic state and effective force concepts to create a nonlocal framework for the analysis of discontinuous deformation and fluid flow in unsaturated porous media (Song and Silling 2020; Menon and Song 2021; Menon and Song 2022c). The governing equations in periporomechanics are integral-differential equations. In this article we use a recently developed updated Lagrangian formulation of periporomechanics, in which it is assumed that each material point x in the current configuration can interact with any other material point x' in its neighborhood, \mathcal{H} . This interaction is termed a bond $\zeta = x' - x$. The bond ζ is the image of the undeformed position vector $\xi = X' - X$ under the deformation, where X' and X are the positions of the x' and x in the undeformed configuration. The neighborhood is a domain of material points around on x that lie within a distance, δ , termed the horizon. The horizon is an explicitly defined length scale parameter, embedded in the global balance laws. In the updated Lagrangian formulation, the horizon remains a uniform sphere independent of the deformation. In light of this, the neighborhood of a material point reads

$$\mathcal{H} = \{x' | x' \in \mathcal{B}, \ 0 \le |\zeta| \le \delta\}$$

where \mathcal{B} denotes a porous body. Under this hypothesis, the material points in the neighborhood can change over time as dictated by their deformation. In this way, the distortion of the horizon in a total Lagrangian formulation under extreme deformation can be avoided. For the notation: boldface represents a vector quantity; bold italics represent a tensor quantity and underscores are used to differentiate peridynamic state quantities from classical point associated quantities. For conciseness, is assumed that a peridynamic state variable without a prime is evaluated at x on the associated bond $\zeta = x' - x$ and the peridynamic state variable with a prime is evaluated at x' on the associated bond $\zeta' = x - x'$.

Under the assumption of passive air pressure, we define the effective force principle as follows (Song and Silling 2020)

$$\underline{\mathscr{T}}[x]\langle \zeta \rangle = \overline{\underline{\mathscr{T}}}[x]\langle \zeta \rangle - S_r \underline{\mathscr{T}}_w[x]\langle \zeta \rangle,$$

where \underline{T} is the total force state, \overline{T} is the effective force state, S_r is the degree of saturation of water, and \underline{T}_w is the fluid force state. It is worth noting that we assume tension is positive for deformation and pore pressure is positive in compression following continuum mechanics convention. Assuming weightless pore air the density of the mixture ρ can be written as

$$\rho = \rho_s(1 - \phi) + S_r \rho_w$$

where ρ_s is the intrinsic density of the solid and ρ_w is the intrinsic density of water, and ϕ is the porosity in the current configuration.

Let u be the displacement vector of material point x in the current configuration. Then, the equation of motion of the updated Lagrangian periporomechanics can be written as

$$\rho \ddot{\boldsymbol{u}} = \int_{\mathscr{H}} (\underline{\mathscr{T}}[\boldsymbol{x}] \langle \underline{\boldsymbol{\zeta}} \rangle - \underline{\mathscr{T}}'[\boldsymbol{x}'] \langle \underline{\boldsymbol{\zeta}}' \rangle) \, d\mathscr{V}' + \rho \boldsymbol{g},$$

where $\underline{\mathscr{T}}$ and $\underline{\mathscr{T}}'$ are the total force vector state at material points \boldsymbol{x} and \boldsymbol{x}' in the current configuration, respectively, $\ddot{\boldsymbol{u}}$ is the acceleration, and \boldsymbol{g} is gravity acceleration vector.

The updated Lagrangian formulation of periporomechanics inherits the material instability of the total Lagrangian formulation (Menon and Song 2021). In this study, we apply the subhorizon concept to avoid the zero-energy mode instability of the original correspondence material models for solid skeleton in the updated Lagrangian periporomechanics. In the horizon of material point x each bond is endowed with a *sub-horizon* composed of material points around the bond that is used to determine the nonlocal deformation gradient, the effective stress and the effective force state on that bond.

We define the sub-horizon \mathcal{H}_s for a bond ζ at material point x as follows

$$\mathcal{H}_s = \mathcal{H} \cap \mathcal{H}'$$
.

For each sub-horizon \mathcal{H}_s , the deformation is represented in rate form using the velocity gradient,

$$\boldsymbol{\mathscr{L}}_s = \left(\int_{\mathscr{H}_s} \underline{\omega} \ \underline{\boldsymbol{\mathscr{Y}}} \otimes \underline{\boldsymbol{\zeta}} \ \mathrm{d} \mathscr{V}' \right) (\boldsymbol{\mathscr{K}}_s)^{-1},$$

using the spatial shape tensor

$$\mathcal{K}_s = \int_{\mathcal{H}_s} \underline{\omega}_{\boldsymbol{\zeta}} \otimes \underline{\boldsymbol{\zeta}} \ \mathrm{d} \mathscr{V}',$$

Given that the sub-horizon rate of deformation tensor reads,

$$oldsymbol{\mathscr{D}}_s = rac{1}{2} [oldsymbol{\mathscr{L}}_s + oldsymbol{\mathscr{L}}_s^T].$$

any classical constitutive material model can be used to relate the rate Cauchy stress $\overline{\sigma}$ to the deformation. Then, following the effective force state concept and the updated Lagrangian correspondence formulation the sub-horizon based total force state reads

$$\underline{\mathscr{T}}_s = \varphi_s \underline{\omega} \ \underline{\zeta} (\mathscr{K}_s)^{-1} (\overline{\sigma}_s - S_r p_w \mathbf{1}).$$

where

$$\varphi_s = \frac{\int_{\mathscr{H}_s} 1 \, d\mathscr{V}'}{\int_{\mathscr{H}} 1 \, d\mathscr{V}'}.$$

The equation of motion for updated Lagrangian sub-horizon correspondence formulation reads

$$\rho \ddot{\boldsymbol{u}} = \int_{\mathcal{H}} \left[\varphi_s \underline{\boldsymbol{\omega}} \ \underline{\boldsymbol{\zeta}} (\boldsymbol{\mathcal{K}}_s)^{-1} (\overline{\boldsymbol{\sigma}}_s - S_r p_w \mathbf{1}) - \varphi_s' \underline{\boldsymbol{\omega}}' \ \underline{\boldsymbol{\zeta}}' (\boldsymbol{\mathcal{K}}_s')^{-1} (\overline{\boldsymbol{\sigma}}_s' - S_r' p_w' \mathbf{1}) \right] \ d\mathcal{V}' + \rho \boldsymbol{g}.$$

The equation of motion is discretized in space via an updated Lagrangian meshfree scheme. In this discretization strategy, a porous continuum material is discretized into a finite number of mixed material points (i.e., solid skeleton and pore water). Assuming a globally drained condition, each material point has one kind of degree of freedom (i.e., displacement) since the pore water pressure (or matric suction) is constant at each material point in the present one-way coupling framework. A uniform grid type discretization is used in this study, such that all mixed points have identical dimensions. At time step *n* the material points in the family of a material point are updated through a search algorithm and each individual neighboring material points is described by their current coordinates. To solve the spatially discretized problem we adopt a central difference explicit time integration scheme (Menon and Song 2022a). For the numerical model, the visco-plastic model for unsaturated soils based critical state concept (Menon and Song 2022b) is adopted for the numerical simulations presented in the following section.

NUMERICAL EXAMPLES

We first study the influence of initial characteristic ratio (radius over height) on the characteristics (e.g., run-out distance and final deposit height) of the soil column collapse under completely dry conditions. Our numerical results are compared with the experimental data in the literature (Lube et al., 2004). We run the simulations with three representative ratios, $a_1 = 0.6$, $a_2 = 1.2$ and $a_3 = 2$. All three specimens have the same initial width $r_0 = 0.1$ m. Figure 1 depicts the three columns considered resting on a rough deformable substrate.

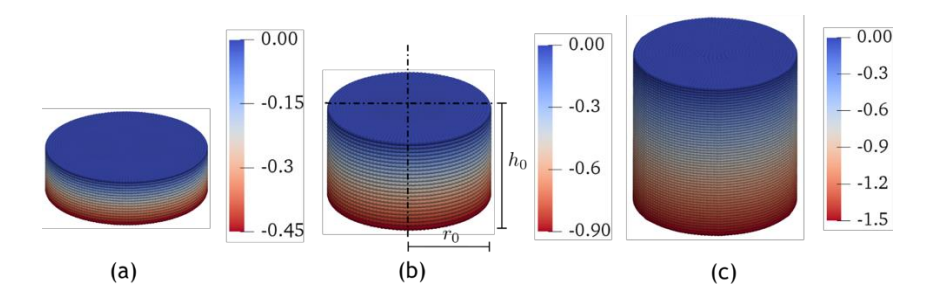


Figure 1. The problem geometry for (a) $a_1 = 0.6$, (b) $a_2 = 1.2$ and (c) $a_3 = 2$ overlaid with contours of initial vertical stress (kPa)

The columns are colored with the contours of the initial vertical stress in the three specimens. The three columns are discretized using 38400, 76800, and 110000 material points, respectively, with uniform mixed points that have a center-to-center distance $\Delta x = 0.0025$ m. The initial geostatic stress in the soil is prescribed through a quasi-static loading step. Subsequently, the lateral constraints on the soil column are relaxed to allow it to collapse onto the rough substrate.

The solid skeleton is modeled using a viscoplastic critical model (Menon and Song, 2022b). The rough substrate is modeled using an isotropic elastic model. For the solid skeleton the

material parameters are: bulk modulus K=25 MPa, shear modulus $\mu_s=15$ Mpa, $\rho_s=2200$ kg/m³, $\rho_w=1000$ kg/m³, initial porosity $\phi_0=0.2$, critical state parameter M=1.1, compression index $\lambda=0.12$, swelling index $\kappa=0.04$, viscoplastic parameter $\eta=1000$ $\frac{Pa^3}{s}$, and an over-consolidation ratio of 1.25 (i.e., slightly overconsolidated soil). The horizon parameter $\delta=0.0075$ m. Additionally, we choose a sub-horizon $\delta'=0.0075$ m to ensure that the sub-horizons for a bond are identical for both end points. Finally, the contact interaction between the soil specimen and the rough substrate is modeled using the short-range force model. In this contact model, contact interactions are modeled using spring-like repulsive forces acting along the normal to the substrate surface. The repulsive forces act between pairs of material points within a cut-off distance of each other $\delta_c=0.002$ m. Their magnitude is proportional to the distance between the contacting points and the contact stiffness $C_f=4MN/m$. Frictional forces are applied as a linear function of the repulsive forces using frictional coefficient $\mu_f=0.2$.

Figure 3, Figure 4 and Figure 5 plot the snapshots of the contours of ε_s^p for the three columns with different a.

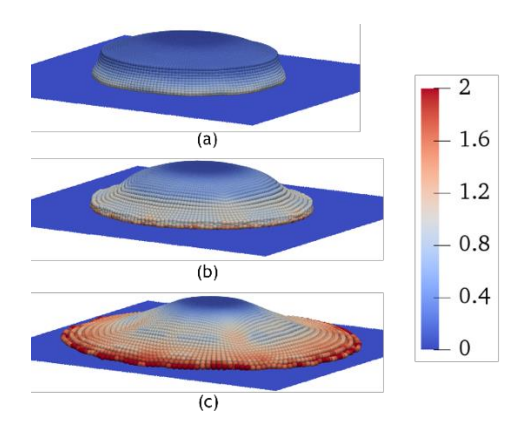


Figure 2. Contours of ε_s^p at (a) t = 0.08 s, (b) t = 0.13 s, (c) t = 0.28 s superimposed on the deformed configuration for $\alpha_1 = 0.6$.

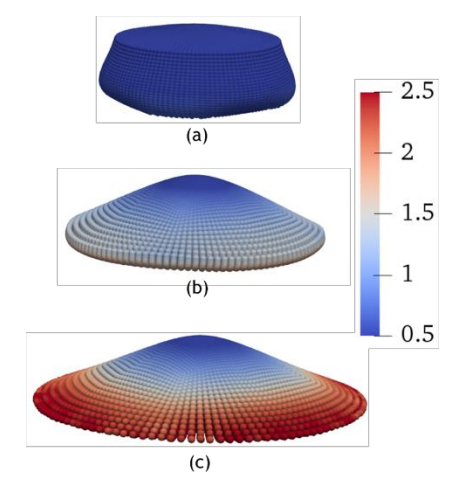


Figure 3. Contours of ε_s^p at (a) t = 0.09 s, (b) t = 0.18 s, (c) t = 0.29 s superimposed on the deformed configuration for $a_2 = 1.2$.

For the shortest column, $a_1 = 0.6$, the collapsing column simply spreads outward from the free surface of the column. As it spreads, the "front" moves inward causing more material to collapse. However, a central column of material is left undisturbed indicated by the dark blue region in the center with no plastic deformation. In Figure 3, we see that for column $a_2 = 1.2$, the flow behavior is similar to the case with $a_1 = 0.6$. The only difference is the final morphology of the deposited material. For this intermediate aspect ratio, the entire column of granular material experiences some deformation. However, the peak height of the collapsed deposit is identical to the initial height of the column. For $a_3 = 2$, the results confirm the existence of two moving layers observed in the experimental testing. Different from the smaller columns, for $a_3 = 2$, the entire column begins moving once the simulation starts. Initially, the results show that the upper half of the column moves directly downward with little horizontal movement, while the base rapidly spreads outward. Subsequently, the upper half of the column moves laterally and creates two lateral moving fronts as seen in (b). Finally, the soil column settles into a deposit with a conical mound at the center surrounded by a wide rim comprised of a very thin layer of soil. This is characteristic of soil columns with large a ($a \ge 2$) as reported in (Lube et al., 2004). The failure behavior and final morphology of the collapsed material correspond to the three flow regimes observed by (Lube et al., 2004; Lajeunesse et al., 2004). In regime 1 ($a \le 0.74$), the collapse resembles quasi-static failure of a soil slope leaving behind a collapsed deposit resembling a truncated cone. In regime 2 (0.74 $\leq a \leq$ 1.7), the collapse propagates to the center of the column leaving a conical deposit. Finally, in regime 3, inertial effects lead to a more spread-out deposited shape.

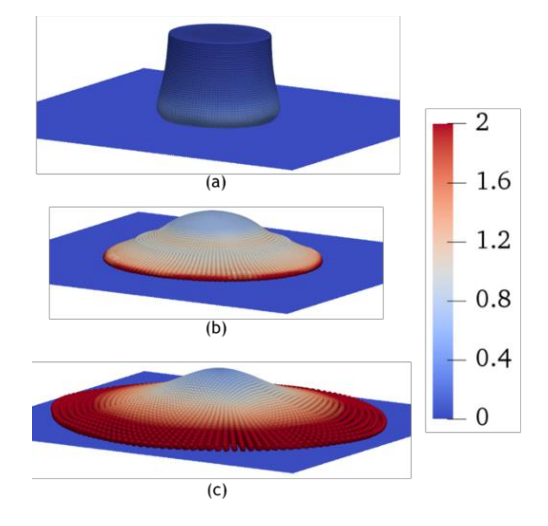


Figure 4. Contours of ε_s^p at (a) t = 0.08 s, (b) t = 0.2 s, (c) t = 0.36 s superimposed on the deformed configuration for $a_3 = 2$.

Next, we examine the influence of initial matric suction on the shape of the final morphology of the collapsed column and the extent of plastic deformation in the soil. Figure 5-Figure 7 plot the contours of equivalent plastic shear strain in the final morphology of collapsed columns with $a_1 = 0.6$, $a_2 = 1.2$, and $a_3 = 2$ for different values of initial matric suction.

The results show that the increase of initial matric suction in the soil column reduces the final runout distance for the same aspect ratio. The final deposit height is generally larger for the specimen with a larger initial matric suction under the same aspect ratio. These observations can

be due to the fact that increasing matric suction generally increases the cohesion of silty soils (Menon and Song 2020, 2021; Fredlund and Rahardjo 1993; Likos et al., 2019).

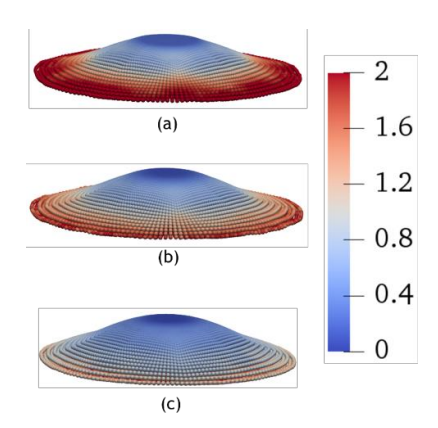


Figure 5. Contours of ε_s^p on the final deposit configuration from simulations with $a_1 = 0.6$ and (a) s = 0, (b) s = 20 kPa and (c) s = 40 kPa.

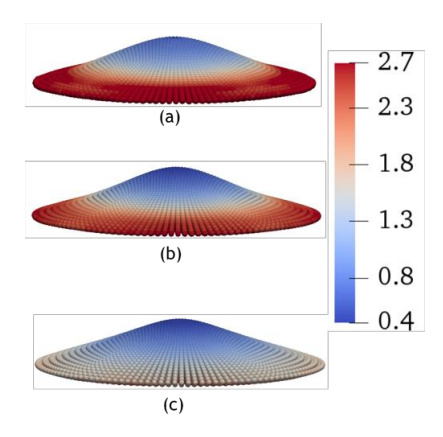


Figure 6. Contours of ε_s^p on the final deposit configuration from simulations with $a_2 = 1.2$ and (a) s = 0, (b) s = 20 kPa and (c) s = 40 kPa.

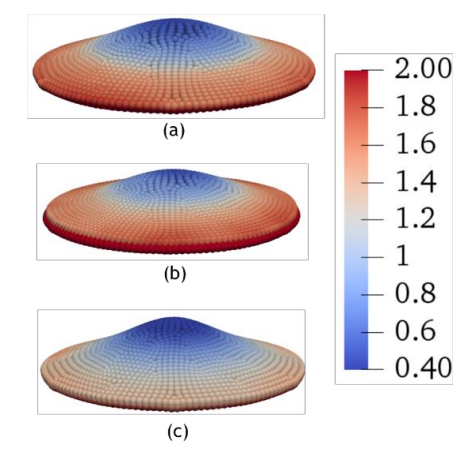


Figure 7. Contours of ε_v^p on the final deposit configuration from simulations using $a_3 = 2$ with (a) s = 0 kPa, (b) s = 20 kPa and (c) s = 40 kPa.

SUMMARY

In this article, we studied the unsaturated soil column collapse under drained conditions (i.e., constant matric suction) through an updated Lagrangian periporomechanics model, which has potential applications in predicting run-out distance of unsaturated slope failure. To validate the proposed periporomechanics, we conducted simulations of three-dimensional soil column collapse in the dry condition using three columns with representative initial aspect ratios. The results showed that the proposed periporomechanics formulation could accurately capture the collapse process observed in the experimental data, for each of the three cases, as well as reproduce the final shape of the collapsed column. Finally, we simulated collapse of unsaturated soil columns with different initial matric suction. In general, the matric suction tended to reduce the run-out of the collapsed column and increase the peak height of the deposited material. Additionally, it is found that the effect of matric suction was more pronounced in columns with larger initial aspect ratio, which deserves further study via a fully coupled periporomechanics framework.

REFERENCES

- Alonso, E. E. (2021). "Triggering and motion of landslides." *Géotechnique*, 71(1), 3-59.
- Fávero Neto, A. H., and Borja, R. I. (2018). "Continuum hydrodynamics of dry granular flows employing multiplicative elastoplasticity." *Acta Geotech.*, 13(5), 1027-1040.
- Fredlund, D. G., and Rahardjo, H. (1993). *Soil mechanics for unsaturated soils*. John Wiley & Sons.
- Lajeunesse, E., Mangeney-Castelnau, A., and Vilotte, J. P. (2004). "Spreading of a granular mass on a horizontal plane." *Phys. Fluids*, 16(7), 2371-2381.
- Likos, W. J., Song, X., Xiao, M., Cerato, A., and Lu, N. (2019). "Fundamental challenges in unsaturated soil mechanics." In *Geotechnical fundamentals for addressing new world challenges* (pp. 209-236). Springer, Cham.
- Lu, N., and Likos, W. J. (2004). *Unsaturated soil mechanics*. Wiley.
- Lube, G., Huppert, H. E., Sparks, R. S. J., and Hallworth, M. A. (2004). "Axisymmetric collapses of granular columns." *J. Fluid Mech.*, 508, 175-199.
- Menon, S., and Song, X. (2020). "Shear banding in unsaturated geomaterials through a strong nonlocal hydromechanical model." *Eur. J. Environ. Civ.*, 26(8), 3357-3371.
- Menon, S., and Song, X. (2021). "A computational periporomechanics model for localized failure in unsaturated porous media." *Comput. Methods Appl. Mech. Eng.*, 384, 113932.
- Menon, S., and Song, X. (2021). "A stabilized computational nonlocal poromechanics model for dynamic analysis of saturated porous media." *Int. J. Numer. Methods Eng.*, 122(20), 5512-5539.
- Menon, S., and Song, X. (2022a). "Computational multiphase periporomechanics for unguided cracking in unsaturated porous media." *Int. J. Numer. Methods Eng.*, 123(12), 2837-2871.
- Menon, S., and Song, X. (2022b). "Updated Lagrangian unsaturated periporomechanics for extreme large deformation in unsaturated porous media." *Comput. Methods Appl. Mech. Eng.*, 400, 115511.

- Menon, S., and Song, X. (2022c). Computational coupled large-deformation periporomechanics for dynamic failure and fracturing in variably saturated porous media. *Int. J. Numer. Methods Eng.*
- Song, X., and Silling, S. A. (2020). "On the peridynamic effective force state and multiphase constitutive correspondence principle." *Journal of the Mechanics and Physics of Solids*, 145, 104161.